Journal of Southeast University (English Edition) Vol. 42, No. 2, pp. 156-164 June 2026 ISSN 1003-7985

Intelligent prediction of long-term tunnel service performance in complex strata via a deep surrogate model

QIN Wenbo[1,2], LUO Hanbin[1,2], LI Yanjin[3], YU Qunzhou[1,2], ZHOU Cheng[1,2]

(1. School of Civil and Hydraulic Engineering, Huazhong University of Science and Technology, Wuhan 430074, China;
2. National Center of Technology Innovation for Digital Construction, Wuhan 430074, China;
3. China Railway Siyuan Survey and Design Group Co., Ltd., Wuhan 430063, China)

Abstract: Tunnels often traverse variable and complex strata, thereby posing significant challenges in analyzing long-term tunnel service performance. This study proposes the tunnel service performance deep surrogate model (TSP-DSM), an intelligent prediction framework designed for predicting long-term tunnel service performance under complex geological conditions. The TSP-DSM framework employs DenseNet as a deep surrogate model, extracting multilevel feature representations from tunnel geological cross-sectional diagrams and horizontal-convergence monitoring data, and adaptively learning the potential nonlinear mapping relationship between geological conditions and service performance. To increase the prediction accuracy, the model's hyperparameters are optimized via random grid search. Experimental results demonstrate that the TSP-DSM achieves a training accuracy of 91.29%, outperforming GoogleNet by 12.79% and ResNet by 5.72%; the prediction performance achieved using grayscale images is comparable to that attained using RGB images. On test samples, which were sourced from complex strata, the TSP-DSM achieves a prediction accuracy of 78.19%, demonstrating strong generalization across various strata. A tunnel service-performance visualization map, constructed based on the intelligent prediction results, provides an intuitive basis for tunnel condition assessment and risk prediction.

Key words: tunnel service performance; tunnel convergence; deep learning; surrogate model; intelligent prediction; complex strata

DOI: 10.3969/j.issn.1003-7985.2026.02.002

The implementation of tunnel engineering heavily relies on a comprehensive understanding of the geological environment in which the tunneling is performed[1]. As urban tunnel infrastructure networks continue to expand, the geological environments encountered in these projects have become increasingly complex, characterized by various strata, including composite layers comprising different types of rocks or soils, and their interactions[2-3]. Variations in load-bearing capacity, deformation characteristics, and permeability between these strata directly affect the design, construction, and operation of tunnels, potentially resulting in structural design deficiencies and heightened construction risks[4-5]. Moreover, challenges such as differential settlement, lining cracks, deformations, and water leakage may arise during the operational phase, jeopardizing the internal environment of the tunnel and undermining the structural reliability thereof[6-8]. Predicting the long-term service performance and resilience of tunnels can assist engineers in assessing their safety, reliability, and recovery capacity under adverse conditions[9-10].

In complex geological strata, predicting the long-term service performance of tunnels poses significant challenges. Comprehensive geological surveys are essential to establish accurate geological data during the early phases of tunnel projects. These surveys yield geological investigation reports, profile diagrams, and other critical outputs that provide a scientific foundation for subsequent design and construction efforts[11-12]. However, these methods heavily rely on the expertise of engineers, necessitating a robust understanding of geological principles and access to extensive project data so as to ensure the precision of design decisions. Furthermore, tunnel projects tend to be large-scale, requiring high-fidelity simulation models throughout the design process, which can be both time-consuming and labor-intensive, thus complicating effective analysis[13-16]. Validating the accuracy of numerical analyses is often challenging[17], which may not completely capture the actual performance of tunnel structures across their long-term service life. Consequently, during the operational phase, engineers predominantly depend on monitoring technologies for fault-based maintenance of tunnel structures, which poses limitations in proactive, effective management of tunnel performance[18-20].

To address these challenges, research on surrogate models has gained increasing prominence in tunnel engi-

Received 2025-08-14, **Revised** 2025-11-13.

Biographies: QIN Wenbo (1993—), male, Ph. D. candidate; ZHOU Cheng (corresponding author), male, doctor, professor, chengzhou@hust.edu.cn.

Foundation item: The National Natural Science Foundation of China (No. 52192664).

Citation: QIN Wenbo, LUO Hanbin, LI Yanjin, et al. Intelligent prediction of long-term tunnel service performance in complex strata via a deep surrogate model[J]. Journal of Southeast University (English Edition), 2026, 42(2): 156-164. DOI: 10.3969/j.issn.1003-7985.2026.02.002.

neering, with the goal of streamlining the prediction process for long-term tunnel service performance[21]. Surrogate models are designed to rapidly forecast tunnel performance by providing more efficient, simplified computational models while maintaining reasonable accuracy[22]. Compared to classical empirical or finite-element approaches, these data-driven surrogates substantially reduce both modeling effort and computational demands. Notably, the integration of deep learning technologies and surrogate models has enhanced traditional approaches by improving areas such as feature extraction and reducing computational complexity.

This study proposes a novel intelligent framework, called the tunnel service performance deep surrogate model (TSP-DSM), designed to predict the long-term service performance of tunnels in complex strata by using a deep surrogate modeling approach. The TSP-DSM automatically extracts latent spatial and mechanical features from geological cross-section diagrams and convergence data, enabling an end-to-end prediction process from geological conditions to service-state classification and generating visualized performance maps that reveal spatial variations in tunnel behavior. This framework provides a scientific foundation for tunnel design and maintenance, allowing engineers to implement preventive measures that enhance the safety and reliability of tunnel structures throughout their service life.

1 Proposed TSP-DSM Framework

The TSP-DSM framework comprises three stages: (1) processing and standardizing geological and monitoring datasets to preserve key physical and structural features; (2) training a deep surrogate model to learn nonlinear mappings between strata characteristics and performance levels; and (3) evaluating predictions via multiple metrics and visualizing results as performance distribution maps, for condition assessment and risk forecasting.

1.1 Processing of geological and monitoring data

1.1.1 Standardization of geological cross-section diagrams

Geological cross-section diagrams are crucial tools in tunnel engineering design, and they are utilized for analyzing and evaluating the composition and structure of strata. These diagrams illustrate the types and thicknesses of various soil and rock layers, which are typically distinguished by different filling patterns, thereby enabling engineers to extract essential geological information that affects tunnel design and safety. A mapping rule correlating geological parameters and grayscale values was developed to enhance the physical information provided to the TSP-DSM. This mapping rule, informed by mechanical parameters such as cohesion C and friction angle φ from survey reports, is expressed as follows:

$$G_{\mathrm{V}} = \boldsymbol{w}^{\mathrm{T}}\begin{bmatrix} C \\ \varphi \end{bmatrix} + b \tag{1}$$

where G_{V} denotes the predicted grayscale value; $\boldsymbol{w}$ denotes the vector of coefficients; and b is a constant term.

Grayscale values were further refined using calculation results and by incorporating expert judgment to avoid excessively similar grayscale values across different strata. Resulting grayscale values, which ranged from 0 to 255, accurately reflected the detailed physical properties of the stratum. Further standardization was required in preparing geological cross-section diagram samples for training the TSP-DSM model. The process (Fig. 1) begins with the transformation of mechanical parameters into grayscale values on the basis of the mapping rule established. The tunnel cross-section diagrams are then rendered using these grayscale values, with areas outside the study scope designated in black (a grayscale value of zero).

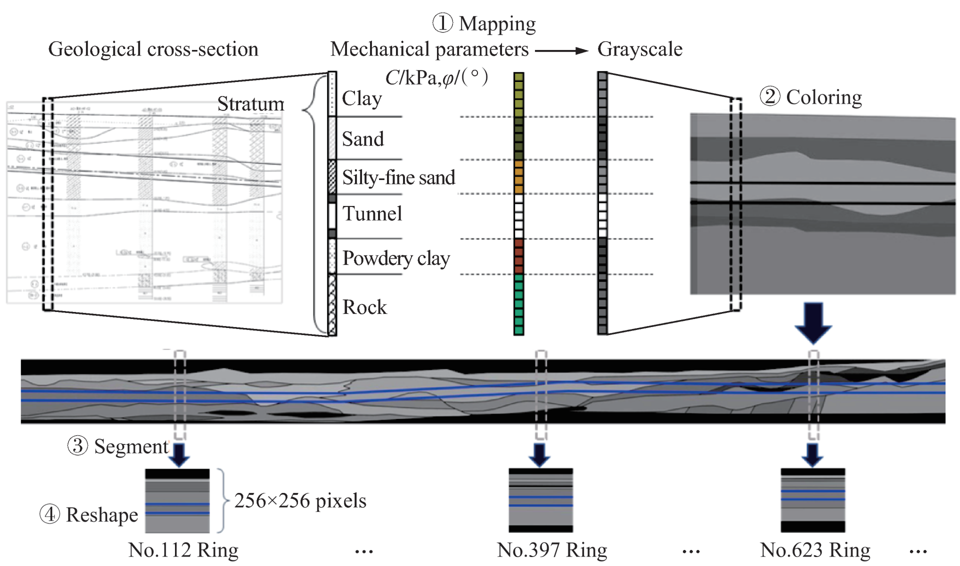

Fig. 1 Workflow for the processing of geological cross-section diagrams

Following this, the diagrams are segmented in accordance with the actual width of tunnel segments and the image pixel scale. Finally, each segmented piece of the diagram is reshaped into a standard sample image size of 256 × 256 pixels, facilitating effective model training and analysis.

1.1.2 Evaluation of long-term service performance

Horizontal convergence was selected as the evaluation metric for assessing the long-term service performance of tunnels. It refers to the radial centripetal contraction of the tunnel structure caused by external pressure and geological influences, and it directly indicates the stress and deformation conditions of the tunnel structure during actual operational states. The workflow for performance assessment based on convergence comprises four steps. Initially, the tunnel point cloud model is preprocessed to eliminate irrelevant points, such as tracks, evacuation passages, and pipelines. The model is then sliced into rings to capture the contour of each tunnel segment. Subsequently, the contours are fitted with ellipses to determine the tunnel center $C(x, y)$ and design diameter d. Subsequently, an arbitrary point P_i is selected on the contour and its distance to $C(x, y)$ is measured as r_i. A second point orthogonal to P_iC is then selected as P_j, and its distance to the tunnel center, r_j, is measured. Two symmetric points located horizontally through the center are selected, denoted by P_h and P_{-h}, and the distance between these two points is measured as r_h. Indicators are calculated as follows:

$$\begin{cases} D_1 = 2\max|r_i - r_j| \\ D_2 = 2\min|r_i - r_j| \\ O = \dfrac{D_1 - D_2}{d} \times 100\% \\ C_h = |r_h - d| \end{cases} \tag{2}$$

where D_1, D_2 denote the major axis and minor axis, respectively; O denotes the ovality; and C_h denotes the horizontal convergence. Finally, a three-level evaluation system for tunnel convergence was developed with reference to GB/T 39559.3—2020 and the project's operation guidelines. As per the standard, the allowable convergence for staggered segmental linings was defined as 0.6%, 0.9%, and 1.2% of the tunnel outer diameter. For the case representing a tunnel with 6 m outer diameter, these values were 36, 54, and 72 mm, respectively. To meet the needs of practical monitoring and risk warning, the four standard grades (0-36 mm (normal), 36-54 mm (attention), 54-72 mm (early warning), and >72 mm (beyond limit)) were simplified into three categories: normal (0-30 mm), early warning (30-50 mm), and beyond limit (>50 mm).

1.2 Deep surrogate model architecture

DenseNet has been selected as the network architecture for the deep surrogate model because of its dense connectivity structure, which enables each layer to directly receive features from all preceding layers. This design effectively mitigates the gradient vanishing problem[23], making it particularly suitable for the processing of high-dimensional geological cross-section diagrams. The architecture's ability to fully leverage abundant feature information is crucial for accurate modeling. Additionally, the parameter growth rate can be adjusted to modify the density of connections within the DenseNet framework. As depicted in a segment of the DenseNet structure in Fig. 2, the output of each layer is concatenated with those of all preceding layers and used as input for subsequent layers.

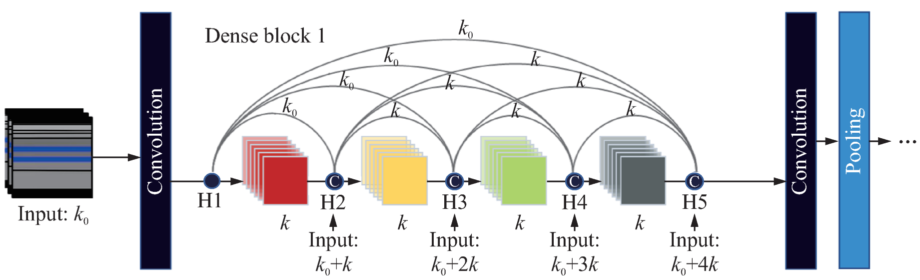

Fig. 2 DenseNet structure

The cross-entropy loss function, offering considerable advantages in accelerating model convergence and enhancing adaptability, has been selected as the scoring function for the training optimization objective. Moreover, the cross-entropy loss possesses inherent adaptability when addressing classification problems, effectively managing probabilistic predictions across the different tunnel-performance grades. The loss function is expressed [24] as follows:

$$H(p, q) = -\sum_{i=1}^{n} p(x_i)\log(q(x_i)) \tag{3}$$

where $p(x_i)$ denotes a binary indicator if class label i is the correct classification for the observation, and $q(x_i)$ denotes the prediction probability of class i.

The cosine decay strategy has been adopted as the learning rate update method. It helps prevent the TSP-DSM from overshooting the optimal solution or becoming ensnared in local minima, thereby allowing the model ample time to learn and to adapt to complex strata conditions. The learning rate update can be illustrated [25] as follows:

$$\alpha_t = \frac{1}{2}\alpha_0\left[1 + \cos\left(\frac{t\pi}{T}\right)\right] \tag{4}$$

where t denotes the current iteration number of the model, and T denotes the preset number of training iterations for the model.

1.3 Evaluation and visualization approach

A comprehensive set of evaluation metrics was selected to assess the effectiveness of the TSP-DSM in predicting "long-term" tunnel service-performance levels. These metrics included a confusion matrix, accuracy, precision, recall, and F1 score. Evaluation metrics offered a comprehensive understanding of the TSP-DSM's predictive performance.

In supervised learning, a confusion matrix is a classic method used to evaluate the performance of classification models, offering not only the counts of misclassifications but also identifying the categories most frequently mispredicted. In a confusion matrix, true positives represent the count of samples correctly predicted as positive, false positives the count of samples incorrectly predicted as positive while actually being negative, false negatives the count of samples incorrectly predicted as negative while actually being positive, and true negatives the count of samples correctly predicted as negative.

Accuracy (A_{cc}) is defined as the ratio of correctly classified samples to the total number of samples, and it reflects the overall effectiveness of the model in "long-term performance" predictions for tunnels:

$$A_{cc} = \frac{T_P + T_N}{T_P + T_N + F_P + F_N} \tag{5}$$

Precision (P_{re}) indicates the proportion of samples that truly belong to a positive class among all those predicted as such by the model, thereby focusing on the model's accuracy in predicting samples with potential long-term performance issues:

$$P_{re} = \frac{T_P}{T_P + F_P} \tag{6}$$

Recall (R_{ec}) measures the proportion of actually positive samples that are correctly predicted by the model, with a high recall indicating the model's effectiveness in capturing potential tunnel-safety hazards:

$$R_{ec} = \frac{T_P}{T_P + F_N} \tag{7}$$

The F1 score (F_1) is the harmonic mean of precision and recall and balances both these metrics:

$$F_1 = \frac{2P_{re}R_{ec}}{P_{re} + R_{ec}} \tag{8}$$

The validation results of the TSP-DSM are shown in Fig. 3, where the performance levels of each segment ring are highlighted in red, yellow, and green. This overlay is automatically applied to geological cross-section diagrams to intuitively display the "long-term tunnel service" performance predicted. This representation enables engineers to quickly identify potential risk areas and segments with weak performance.

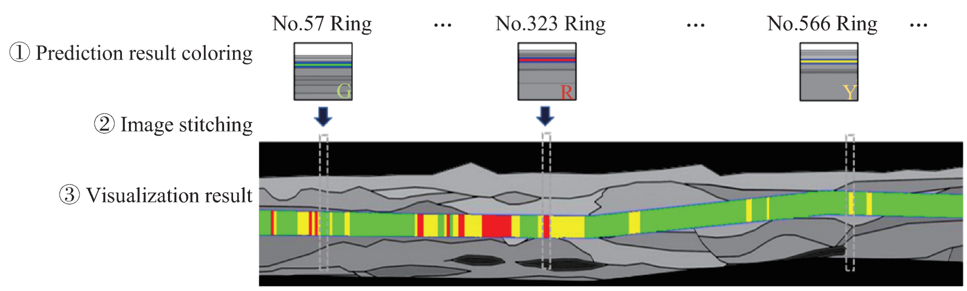

Fig. 3 Visualization of prediction results

2 TSP-DSM Implementation and Evaluation

2.1 Data acquisition and preparation

The data utilized herein were derived from a metro line that began operations in 2012[26]. This metro line comprises 20 sections, each consisting of left and right tunnels. Notably, 14 of these sections were constructed using shield tunneling techniques. To maintain consistency in the research data, only shield sections were selected for analysis. The results for tunnel horizontal convergence (according to the 2021 monitoring report issued by the metro operation company) are shown in Fig. 4, the proportions of different convergence warning levels for the left-line and right-line tunnels are denoted by P_L and P_R, respectively, while the corresponding horizontal convergence values are represented by C_L and C_R. The sections from C-H to X-J are mainly located within the first-level terrace along the Yangtze River and exhibit the most severe convergence deformation, with exceedance ratios ranging from 20% to 65%. In response to these findings, the tunnel operation administration implemented measures such as reinforcement using steel plates to mitigate the issues encountered.

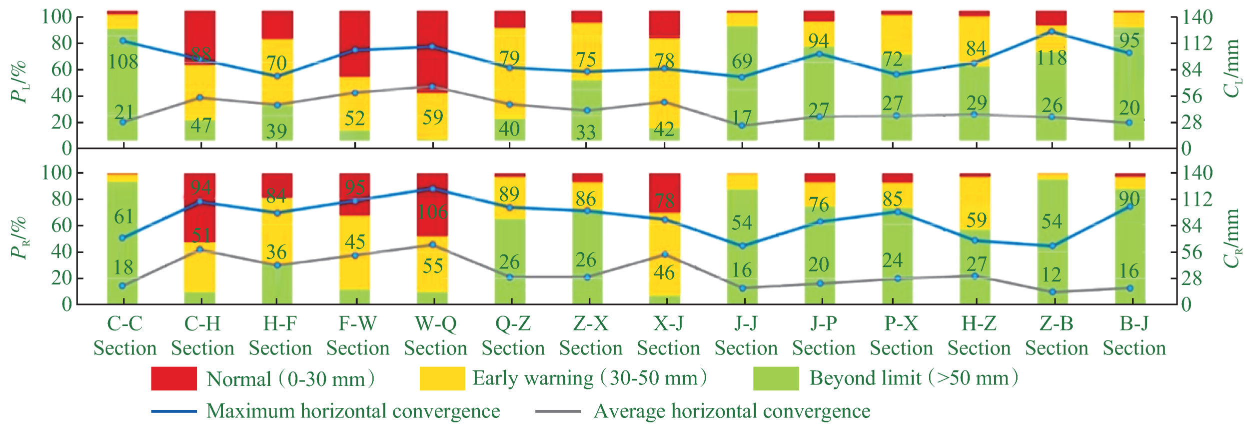

Fig. 4 Distribution of tunnel convergence under various geological conditions

The monitoring report details information for each segment ring, encompassing ring number, mileage, and convergence value. After excluding data anomalies caused by obstructions such as electrical boxes, a total of 9 177 samples from the left tunnels and 8 989 samples from the right tunnels were collected. Following the previously outlined standardization process (Section 1.1.2), the convergence monitoring data and geological cross-section diagrams yielded a total of 9 851 normal samples (green), 5 349 early-warning samples (yellow), and 2 966 beyond-limit samples (red). To ensure a balanced representation of the three categories during training, an undersampling strategy was applied to both the green and yellow samples. Approximately 35% of normal samples were randomly removed through an undersampling procedure, ensuring that each category contained a comparable number of training instances. To validate the generalizability of the TSP-DSM, data from the B-J Section were used as an independent test set. This 1.2-km, left-line shield tunnel (diameter 6.0 m, average depth 15.4 m) provided representative soft-hard interbedded geological conditions for validation.

2.2 Training and hyperparameter selection

The DenseNet architecture employed in the TSP-DSM delivered high performance while using fewer hyperparameters, making it well-suited for training on relatively limited sample sizes. Four hyperparameters were selected for the tuning process (Table 1).

Table 1 Hyperparameter random grid search configuration

Hyperparameter	Range
Growth rate r_g	16, 32, 64
Learning rate r_l	Min:1×10^{-6}; max:0.01
Learning rate factor f_{lr}	0.01, 1×10^{-4}, 1×10^{-6}
Epochs	Min:50; max:200; step:50

Hyperparameters for the TSP-DSM can be predetermined using specific values before training commences. The random grid search method was implemented for automatic parameter tuning. This approach randomly samples from the parameter subspace, controlling the number of parameter combinations by constraining the search space.

Among all tested parameter combinations, the optimal configuration was obtained with a growth rate r_g of 32, a learning rate r_l of 8.863×10^{-5}, a learning rate factor f_{lr} of 1×10^{-6}, and 200 training epochs. After identifying this optimal configuration, the model was retrained on the full training dataset; the model eventually attained a training loss of 0.169 7 and an accuracy of 91.29% on the training set. The training process is shown in Fig. 5.

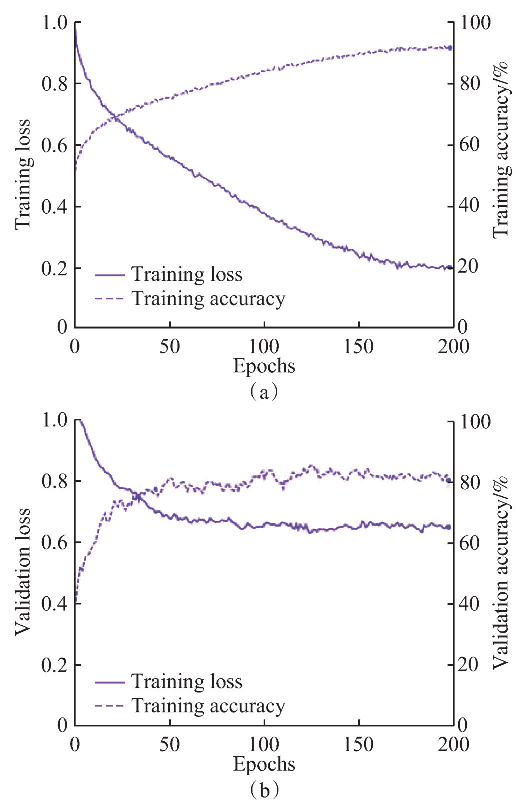

Fig. 5 Training and validation processes of the optimal hyperparameter combination. (a) Training process; (b) Validation process

2.3 Prediction result analysis and visualization

Following the selection of the model's optimal hyperparameters, its prediction capabilities for long-term tunnel service performance levels were evaluated. A confusion matrix was constructed to assess the model's training effectiveness. From the existing training set, a total of 1 000 samples were extracted, comprising 400 normal samples (green), 300 early-warning samples (yellow), and 300 beyond-limit samples (red). These samples were then combined to create a new dataset for prediction. The model's prediction results are detailed in Fig. 6.

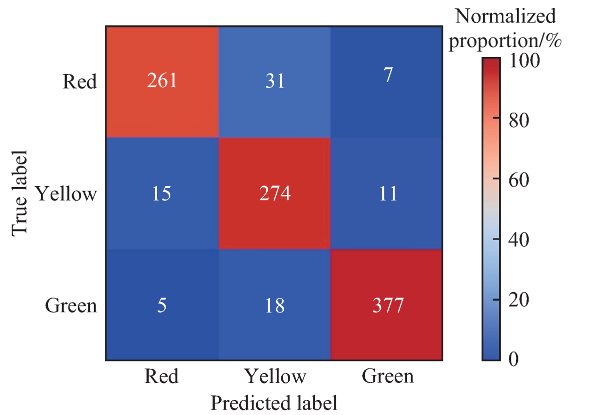

Fig. 6 Confusion matrix of the prediction model on the training set

The results shown in Fig. 6 indicate that the prediction accuracy on trained samples exceeded 91%. The model achieved the highest prediction accuracy on normal samples, followed by the accuracy on beyond-limit samples, with the accuracy on both categories being larger than 92%. However, the prediction accuracy on early-warning samples was lower, about 85%. A detailed analysis of these prediction results revealed that the two most common prediction errors were instances where actual beyond-limit samples were misclassified as early-warning samples and instances where actual normal samples were misclassified as early-warning ones. Only a small fraction of samples exhibited confusion between the beyond-limit and normal categories.

The highest recall value was achieved on normal samples, followed by that on early-warning samples, with the lowest recall value attained on beyond-limit samples. This trend indicated that the model exhibited superior predictive accuracy for normal segment rings under actual convergence-deformation conditions. As monitoring data from engineering practices are inherently imbalanced, the dataset used notably influenced the effectiveness of the TSP-DSM; specifically, the proportion of measurement points in high-risk states is moderately limited in actual operational tunnels. This imbalance was the primary factor contributing to the model's inadequate prediction of beyond-limit samples.

To assess the model's generalizability, the left-line tunnel data were reserved as the test dataset. The prediction results of the TSP-DSM on the test dataset are presented in Fig. 7. The calculated accuracy and recall values were low owing to the extreme imbalance in the number of samples across different categories within the test dataset, failing to accurately represent the predictive performance of the TSP-DSM. Therefore, accuracy was selected as the basis for evaluating the model's generalizability. After training the saved model using the previously determined parameter combinations, it achieved an accuracy of 78. 19% on the test set, which was slightly lower than that recorded on the validation set during model training. Overall, the prediction accuracy remained limited for entirely new strata that had not been previously encountered during training.

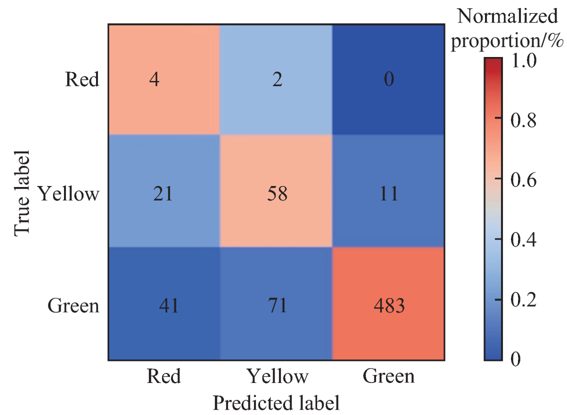

Fig. 7 Evaluation of the model's generalizability on the test set

Further processing of prediction results involves the integration of generated labels and the corresponding positions of tunnel segments. Different performance levels are represented using RGB colors on geological cross-section diagrams. This approach produces a comprehensive map that visualizes the distribution of predicted long-term service performance across the entire tunnel. The results are shown in Fig. 8. The prediction results closely matched the measured labels, with green, yellow, and red zones indicating normal, early-warning, and beyond-limit convergence regions along the tunnel alignment, respectively.

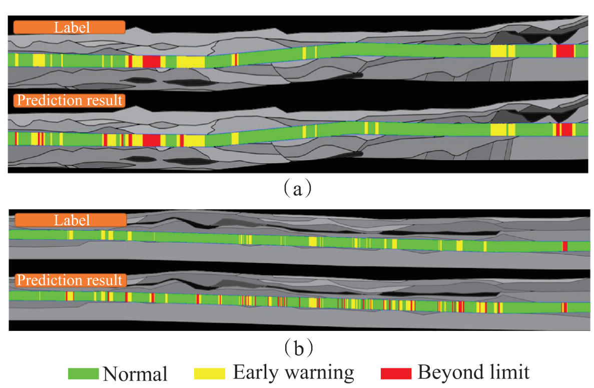

Fig. 8 Prediction distribution map of long-term tunnel service performance. (a) Visualization on training set; (b) Visualization on test set

3 Discussion

3.1 Effect of network architecture on TSP-DSM performance

Geological cross-sectional diagrams are inherently less complex than general image recognition tasks. Accordingly, the performances of three widely used network architectures—ResNet, GoogleNet, and DenseNet—were evaluated within the TSP-DSM framework. ResNet effectively propagates gradients in deep networks through residual connections, facilitating easier optimization and training [27]. GoogleNet extracts multiscale features by using various convolutional kernels, then integrating these features to achieve a more accurate and comprehensive representation [28]. ResNet addresses the issue of gradient vanishing in deep networks by exploring depth, while the inception modules of GoogleNet explore width. DenseNet emphasizes the maximization of feature utilization, resulting in enhanced performance and parameter efficiency. The initial hyperparameters were set to 200 epochs, a batch size of 8, a learning rate r_l of 1×10^{-4}, and a learning rate factor f_{lr} of 1×10^{-6}. The training records of the three optimized TSP-DSM models after parameter tuning are shown in Fig. 9.

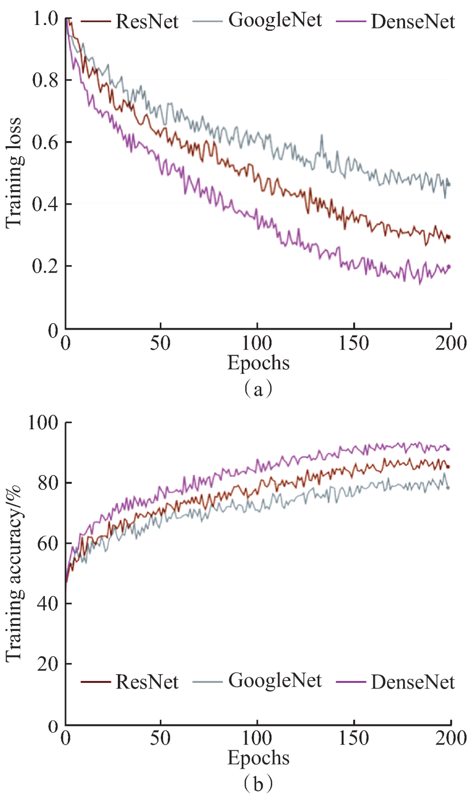

Fig. 9 Comparison of training processes between various network architectures. (a) Training loss; (b) Training accuracy

Table 2 compares the training results for the three TSP-DSMs. Among the three network architectures, DenseNet delivered the best performance by achieving the lowest training loss and highest accuracy, recorded at 0.169 7 and 91.29% (at the end of 200 epochs), respectively. This indicated that the feature-reuse and layer-by-layer connectivity mechanisms of DenseNet were highly effective for tasks involving geological cross-sectional diagrams, facilitating more efficient parameter utilization. Although GoogleNet and ResNet possessed merits such as multiscale processing and effective training for deep networks, they did not perform as effectively as DenseNet for this specific task.

Table 2 Comparison of training results between different network architectures

Network architecture	DenseNet	GoogleNet	ResNet
Training loss	0.169 7	0.461 8	0.291 6
Training accuracy/%	91.29	78.77	85.84

3.2 Effect of color mode on TSP-DSM performance

Datasets with distinct color libraries were established to assess the effect of different color modes on training results: an RGB color library using three channels and a grayscale library utilizing a single channel. The grayscale library has been previously detailed, while the RGB library was developed based on geological map color conventions, with stratum numbers organized according to geological eras and their corresponding color mappings. Organizing stratum numbers in conjunction with color mappings based on geological eras. Color images, which convey more information across the three channels, typically yield improved training results in various image processing tasks. However, the differ-

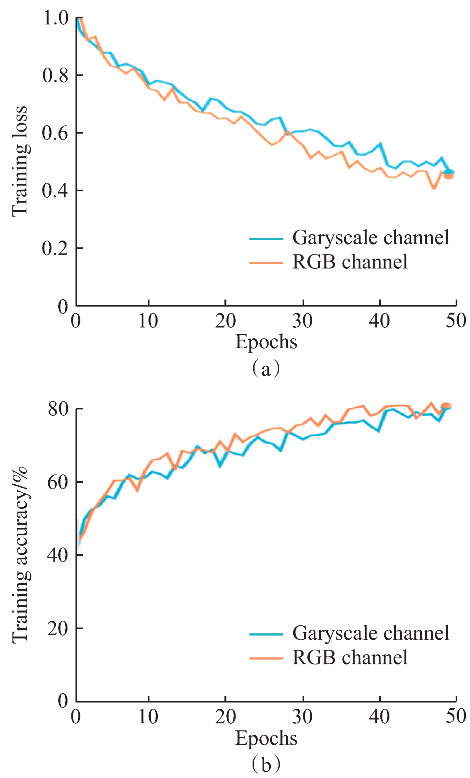

Fig. 10 Comparison of training processes between RGB and grayscale samples. (a) Training loss; (b) Training accuracy

ences in training results between the two color modes were smaller than 1% (Fig. 10). The final test accuracies were 78.19% (grayscale) and 78.41% (RGB); additionally, a McNemar's test yielded a *p*-value larger than 0.05, confirming that the difference was not statistically significant. This minimal discrepancy suggested that grayscale images adequately represented geological information for neural network training, likely producing feature vectors comparable to those generated from color images. Conversely, we can say that employing single-channel grayscale images simplifies the sample preparation process, reduces data transmission and storage costs, and decreases model complexity and training expenses.

4 Conclusions

(1) This study developed TSP-DSM, an intelligent framework for the prediction of long-term tunnel service performance. Through rigorous testing and analysis, the TSP-DSM elucidated the implicit nonlinear relationships between complex strata and long-term tunnel service performance on the basis of tunnel-convergence evaluations, providing end-to-end prediction capabilities. The proposed framework was validated for shield tunnels, and its conclusions would apply to similar monitoring and construction conditions.

(2) A method for constructing a geological cross-section diagram dataset was developed, along with investigating the effect of color channels on model training. The results indicated that the training-performance difference between RGB and grayscale images was within 1%, thereby confirming the effectiveness of using grayscale images in simplification of prediction tasks.

(3) The effect of hyperparameters on model training was analyzed by utilizing an automatic hyperparameter-tuning approach based on random grid search. The optimal parameter combination for the TSP-DSM was obtained with a growth rate r_g of 32, a learning rate r_l of 8.863×10^{-5}, a learning rate factor f_{lr} of 1×10^{-6}, and 200 training epochs. The training results demonstrated a prediction accuracy of 91.29% on the training set and 78.19% on the test dataset.

(4) The capabilities of three mainstream deep learning network architectures were assessed within the TSP-DSM framework. A comparative analysis identified DenseNet as the most effective architecture, delivering the highest predictive performance. In accuracy, DenseNet outperformed GoogleNet by 12.79% and ResNet by 5.72%.

(5) The proposed TSP-DSM achieved a test accuracy of 78.19%, acceptable for early-warning and auxiliary assessment in practice; this performance indicated a certain degree of generalizability under heterogeneous ground conditions, as the dataset had been collected from an over 20 km metro line traversing diverse strata. Future work would extend validation across multiple lines and geological regions and explore transfer-learning or data-fusion strategies to enhance robustness and scalability.

References

[1] ZHANG W G, SOMERVILLE I, PANEIRO G, et al. Design and construction of tunnels and tunnelling: Understanding the importance of geological conditions, landslide susceptibility and risk assessment[J]. Geological Journal, 2024, 59(9): 2365-2370.

[2] FU K, QIU D H, XUE Y G, et al. TBM tunneling strata automatic identification and working conditions decision support [J]. Automation in Construction, 2024, 163: 105425.

[3] XU Z W, ZHANG C, ZHOU S H, et al. GFNS: An OpenGL-based tool for shield tunneling simulation in 3D complex stratum[J]. Computers and Geotechnics, 2024, 167: 106111.

[4] WANG K, XU S S, ZHONG Y J, et al. Deformation failure characteristics of weathered sandstone strata tunnel: A case study [J]. Engineering Failure Analysis, 2021, 127: 105565.

[5] ZHANG S L, GAO J L, LIU C, et al. Model test on the collapse mechanism of subway tunnels in the soil-sand-rock composite strata[J]. Engineering Failure Analysis, 2024, 162: 108356.

[6] YU T S, ZHANG Y X, YAN Z G. A new generation method of tunnel progressive defect status random field (TPDSRF) for subway tunnel structure[J]. Tunnelling and Underground Space Technology, 2023, 141: 105340.

[7] LI Z Z, WANG H, CHANG X Y, et al. Prediction of surrounding rock convergence deformation of high-speed railway tunnel based on combined model[J]. Journal of Southeast University (Natural Science Edition), 2021, 51(5): 851-858. (in Chinese)

[8] ZHANG Z G, MAO M D, ZHANG C P, et al. Analysis on viscoelastic soil consolidation settlement of fractional order induced by tunnel leakage[J]. Journal of Southeast University (Natural Science Edition), 2022, 52(3): 530-537. (in Chinese)

[9] BELLINI MACHADO L, MASSAO FUTAI M. Tunnel performance prediction through degradation inspection and digital twin construction[J]. Tunnelling and Underground Space Technology, 2024, 144: 105544.

[10] SHI C, WANG Y. Development of subsurface geological cross-section from limited site-specific boreholes and prior geological knowledge using iterative convolution XGBoost[J]. Journal of Geotechnical and Geoenvironmental Engineering, 2021, 147(9): 04021082.

[11] GAN B L, ZHANG D M, HUANG Z K, et al. Ontology-driven knowledge graph for decision-making in resilience enhancement of underground structures: Framework and application [J]. Tunnelling and Underground Space Technology, 2025, 163: 106739.

[12] CARTER T G, BARNETT W P. Improving reliability of structural domaining for engineering projects [J].

Rock Mechanics and Rock Engineering, 2022, 55(5): 2523-2549.

[13] GUO Z Z, QIU D H, YU Y H, et al. Analysis and prediction of nonuniform deformation in composite strata during tunnel excavation[J]. Computers and Geotechnics, 2023, 157: 105338.

[14] QIU J T, ZHOU X J, SHEN Y S, et al. Failure mechanism of the deep-buried metro tunnel in mixed strata: Physical model test and numerical investigation[J]. Tunnelling and Underground Space Technology, 2023, 139: 105224.

[15] LIU Z H, FANG Q, SHEN Y, et al. Two-stage surrogate modeling strategy for predicting foundation pit excavation-induced strata and tunnel deformation [J]. Tunnelling and Underground Space Technology, 2024, 151: 105845.

[16] WANG F, ZENG J P, FANG Y B, et al. Research on the mechanism of deformation of tunnel lining structure exposed to fire based on transient thermal strain[J]. Journal of Southeast University (Natural Science Edition), 2025, 55(3): 856-863. (in Chinese)

[17] POTTS D M. Numerical analysis: A virtual dream or practical reality?[J]. Géotechnique, 2003, 53(6): 535-573.

[18] ZHANG J Z, PHOON K K, ZHANG D M, et al. Deep learning-based evaluation of factor of safety with confidence interval for tunnel deformation in spatially variable soil[J]. Journal of Rock Mechanics and Geotechnical Engineering, 2021, 13(6): 1358-1367.

[19] ZHANG J Z, PHOON K K, ZHANG D M, et al. Novel approach to estimate vertical scale of fluctuation based on CPT data using convolutional neural networks[J]. Engineering Geology, 2021, 294: 106342.

[20] ZHANG H L, LUO F, GENG W J, et al. An efficient method for reliability analysis of high-speed railway tunnel convergence in spatially variable soil based on a deep convolutional neural network[J]. International Journal of Geomechanics, 2023, 23(11): 04023210.

[21] QIN W B, CHEN E J, WANG F, et al. Data-driven models in reliability analysis for tunnel structure: A systematic review[J]. Tunnelling and Underground Space Technology, 2024, 152: 105928.

[22] ALIZADEH R, ALLEN J K, MISTREE F. Managing computational complexity using surrogate models: A critical review [J]. Research in Engineering Design, 2020, 31(3): 275-298.

[23] HUANG G, LIU Z, VAN DER MAATEN L, et al. Densely connected convolutional networks [C]//2017 IEEE Conference on Computer Vision and Pattern Recognition (CVPR). Honolulu, HI, USA, 2017: 2261-2269.

[24] MAO A Q, MOHRI M, ZHONG Y T. Cross-entropy loss functions: Theoretical analysis and applications [C]// International Conference on Machine Learning. Honolulu, HI, USA, 2023, 202: 23803-23828.

[25] LOSHCHILOV I, HUTTER F. SGDR: Stochastic gradient descent with warm restarts[EB/OL]. (2016-08-13)[2025-08-10]. https://doi. org/10. 48550/arXiv. 1608. 03983.

[26] ZHOU C, QIN W B, LUO H B, et al. Digital twin for smart metro service platform: Evaluating long-term tunnel structural performance[J]. Automation in Construction, 2024, 167: 105713.

[27] HE K M, ZHANG X Y, REN S Q, et al. Deep residual learning for image recognition[C]//2016 IEEE Conference on Computer Vision and Pattern Recognition (CVPR). Las Vegas, NV, USA, 2016: 770-778.

[28] SZEGEDY C, LIU W, JIA Y Q, et al. Going deeper with convolutions[C]//2015 IEEE Conference on Computer Vision and Pattern Recognition (CVPR). Boston, MA, USA, 2015: 1-9.

基于深度代理模型的复杂地层隧道长期服役性能智能预测

覃文波[1,2], 骆汉宾[1,2], 李彦锦[3], 余群舟[1,2], 周诚[1,2]

(1.华中科技大学土木与水利工程学院,武汉 430074;2.国家数字建造技术创新中心,武汉 430074;
3.中铁第四勘察设计院集团有限公司,武汉 430063)

摘要: 复杂多变的地层环境给隧道长期服役性能分析带来了显著挑战。为此,本研究提出一种名为隧道服役性能深度代理模型(TSP-DSM)的智能预测框架,用于在复杂地质条件下预测隧道长期服役性能。TSP-DSM采用DenseNet作为深度代理模型,能够从隧道地质剖面图与水平收敛监测数据中提取多层特征表示,自适应学习地质条件与服役性能之间潜在的非线性映射关系。为提升预测精度,模型超参数采用随机网格搜索进行优化。实验结果表明:TSP-DSM在训练集上的预测准确率达到91. 29%,较GoogleNet与ResNet分别提升12. 79%和5. 72%;灰度图像与RGB图像在预测精度上表现相近。TSP-DSM在测试集中预测准确率为78. 19%,表现出在复杂地层条件下较强的泛化能力。基于智能预测结果构建的隧道服役性能可视化分布图,能够为隧道状态评估与风险预判提供直观依据。

关键词: 隧道服役性能;隧道收敛;深度学习;代理模型;智能预测;复杂地层

中图分类号: TU17